

The Optical Spectrum of Single-Crystal $(\text{CH}_3\text{NH}_3)\text{PbBr}_3$ Cleaved in Ultrahigh Vacuum

Daniel Niesner,^{1,*} Oskar Schuster,¹ Max Wilhelm,¹ Ievgen Levchuk,² Andres Osvet,² Shreetu Shrestha,² Miroslaw Batentschuk,² Christoph Brabec,^{2,3} and Thomas Fauster¹

¹*Lehrstuhl für Festkörperphysik, Friedrich-Alexander-Universität Erlangen-Nürnberg (FAU), Staudtstr. 7, 91058 Erlangen, Germany*

²*Institute of Materials for Electronics and Energy Technology (I-MEET),*

Department of Materials Science and Engineering,

Friedrich-Alexander-Universität Erlangen-Nürnberg (FAU), Martensstrasse 7, 91058 Erlangen, Germany

³*Bavarian Center for Applied Energy Research (ZAE Bayern), Haberstrasse 2a, 91058 Erlangen, Germany*

(Dated: March 11, 2019)

To explore the intrinsic optical properties of $(\text{CH}_3\text{NH}_3)\text{PbBr}_3$, we measure temperature-dependent one-photon and two-photon induced photoluminescence from single crystals cleaved in ultrahigh vacuum. Comparison of the two allows to identify defect emission and to extract absorption spectra, when diffusion is taken into account. We find two optical transitions: a direct one at an energy of 2.31 eV independent of temperature, and an indirect one at 2.25 eV (2.22 eV) in the orthorhombic (tetragonal) phase. The spectra are consistent with Rashba-type spin-splittings in the band structure by 60 meV (90 meV). Each transition is accompanied by an excitonic transition \approx 22 meV lower in energy. In the cubic phase, the binding energy of the exciton related to the direct transition is smaller. Excitonic emission associated with the indirect transition redshifts, possibly because of phononic effects. High-energy emission from free carriers is observed with higher intensity than reported in earlier studies. It disappears after exposure to air.

Organic-inorganic perovskite semiconductors (OIPS) have opened a whole new field in optoelectronics [1–7]. A comprehensive understanding of the underlying photophysics is still under development. Therefore, detailed knowledge is required of the band structure of OIPS [8–12], modifications by local disorder [13–18], excitonic effects [19–24], polaronic screening [25–28], and their interplay. Many studies that tackle these questions rely on the interpretation of (time-resolved) optical spectroscopy. Experimental data and their interpretation, however, show strong variations. Spectroscopic results obtained from thin films depend on growth technique [29–33], grain size [30, 34], and environmental conditions [35, 36].

For example, exciton binding energies between 15 and 84 meV [23, 37–42] have been reported for $(\text{CH}_3\text{NH}_3)\text{PbBr}_3$. A recent study on lead-bromide single-crystals found photoluminescence (PL) from high-energy carriers [28] with the potential to enhance solar cell performance, possibly beyond the Shockley-Queisser limit [43]. High-energy carriers have not been apparent to the same degree in earlier studies on thin films. Polaron formation involving reorientation of the organic molecules was proposed as the mechanism that suppresses electron-phonon scattering [28]. A recent study found a double peak structure with a peak spacing of 60 meV in the PL spectrum of $\text{CH}_3\text{NH}_3\text{PbI}_3$ [44]. From pressure-dependent experiments the authors identified direct and indirect optical transitions in the presence of Rashba-type spin-splitting as the origin of the two peaks. Rashba-type spin splitting has been predicted for $\text{CH}_3\text{NH}_3\text{PbBr}_3$ as well [8, 29, 45, 46], and

we recently confirmed it experimentally using surface-sensitive photoelectron spectroscopy [47]. In PL from $\text{CH}_3\text{NH}_3\text{PbBr}_3$, a similar double-peak structure is thus expected as in case of $\text{CH}_3\text{NH}_3\text{PbI}_3$. Previously, two PL peaks at 2.22 eV and 2.3 eV were attributed to phases with lower and higher band gap in the bulk and surface-near region of $\text{CH}_3\text{NH}_3\text{PbBr}_3$ [48]. Yet, measurements in the surface-near region of OIPS are particularly challenging, since the crystals are extremely sensitive to environmental gas adsorption [35].

To access intrinsic material properties, we perform steady-state PL spectroscopy at low excitation density on surfaces of $(\text{CH}_3\text{NH}_3)\text{PbBr}_3$ single crystals cleaved in ultrahigh vacuum (UHV). These surfaces emit broadband PL light. We also measure bulk-sensitive steady-state PL spectra induced by two-photon absorption (TPI-PL). Because of the vastly different excitation depths, absorption spectra can be extracted from the combination of PL and TPI-PL when diffusion is taken into account. The procedure poses a viable route to extend temperature-dependent optical absorption spectroscopy to single crystals. We find a prominent direct transition at a photon energy of 2.31 eV, and an indirect transition slightly lower in energy. The transitions can be assigned to Rashba-type spin-split bands. Their spacing increases from 60 meV to 90 meV as $(\text{CH}_3\text{NH}_3)\text{PbBr}_3$ undergoes its phase transition from the orthorhombic to the tetragonal structure at 150 K. Each transition is accompanied by an exciton with a binding energy of \approx 22 meV at temperatures \leq 200 K. In the high-temperature cubic phase, the binding energies of the two excitons show opposite trends. In addition, we observe intense high-energy PL

emission from free carriers in single crystals cleaved in UHV. Possible origins of the observed features and trends are discussed. The data pose an important step towards a complete understanding of the optical properties of OIPS, and can serve as a reference for various future spectroscopic and theoretical studies.

Details of crystal growth, characterization, and preparation are given in Ref. [47]. Cleaving in UHV is used to create surfaces of $(\text{CH}_3\text{NH}_3)\text{PbBr}_3$ single crystals with bulk-terminated surface-Brillouin zone [47] and atomic arrangement [49]. The photoluminescence experiments are illustrated in Fig. 1 (a). For 405 nm excitation, a cw laser source was used with an intensity of 0.3 W/cm^2 , comparable to the total terrestrial intensity of solar irradiation. The PL spectra from surfaces cleaved in UHV show distinct differences to the ones of air-exposed crystals and are much broader, see Fig. 1 (b). This broad emission spectrum forms the basis for the further analysis presented in this letter.

The PL signal stimulated by 800 nm below band-gap excitation, Figs. 1 (c) and (d), is the result of two-photon absorption. We use a high repetition-rate laser (4.2 MHz) and low pulse energy (2 nJ) to ensure steady-state conditions, see Ref. [50] for details. With the applied excitation density of $1 \cdot 10^{13} \text{ cm}^{-3}$ absorbed photons per pulse the penetration depth (5 mm) of the laser is longer than the thickness of the crystals ($1.3 \pm 0.3 \text{ mm}$). The excitation density is sufficient to saturate defects that are most obvious in the low-temperature orthorhombic phase of OIPS. Fig. 1 (c) shows TPI-PL spectra of orthorhombic $(\text{CH}_3\text{NH}_3)\text{PbBr}_3$, normalized to the square of the laser fluence, which reflects the excitation density. The low energy ($< 2.16 \text{ eV}$) part of the spectrum saturates quickly. We thus attribute the signal to defects. In contrast, as the light intensity is increased, the signal from the higher-energy TPI-PL emission feature first increases quadratically in laser fluence, and then with the fourth power, see also Fig. 1 (d). We ascribe the quadratic behavior (linear in excitation density) to excitonic and/or defect recombination, and the fourth-power dependence (quadratic in excitation density) to free carrier recombination. Spectra shown in this paper were recorded with excitation densities beyond the onset of free-carrier emission, with possible defects saturated. The integral intensity of the room-temperature TPI-PL spectrum is given in Fig. 1 (d) as well. The signal increases with the fourth power of laser fluence (quadratically in excitation density) down to the lowest TPI-PL intensities we can detect, indicating free-carrier recombination.

In Fig. 2 (a) we compare steady-state PL spectra with excitation wavelengths of 405 nm (blue) and 800 nm (red) for various temperatures. TPI-PL spectra are narrow with an asymmetric shape. The main emission occurs at lower energy than that of regular PL. We fit TPI-PL spectra using the sum of two Voigt functions T0 and T1 (dark red lines). Resulting peak positions

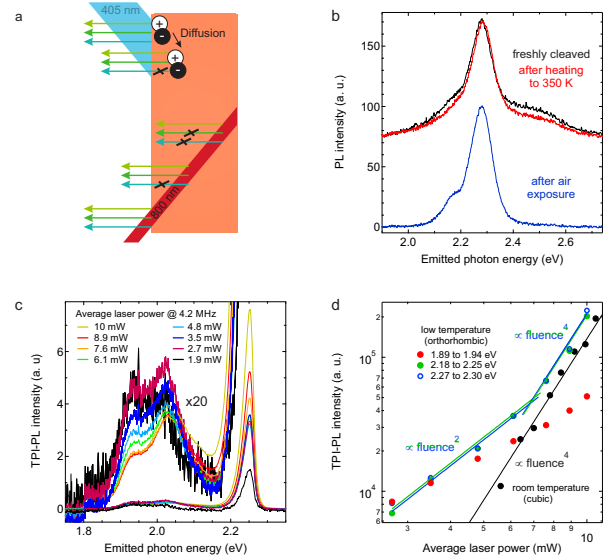


FIG. 1: Conventional PL and TPI-PL from $(\text{CH}_3\text{NH}_3)\text{PbBr}_3$. (a) illustrates absorption of 405 nm and 800 nm, and reabsorption resulting from the long penetration depth of infrared light. In (b) PL spectra measured under different environmental conditions are compared. (c) shows intensity-dependent TPI-PL data from the low-temperature orthorhombic phase, normalized to the second power of the incoming laser flux. Intensities in selected spectral regions, as well as the integral TPI-PL intensity at room temperature are given in (d).

are indicated by vertical lines. Fit results are summarized in Fig. 3. Two-photon absorption at wavelengths around 800 nm resembles one-photon absorption at half the wavelength [51], without being affected by real intermediate states or one-photon absorption. Therefore the PL emission following one-photon absorption at 405 nm and two-photon absorption at 800 nm should be almost identical for sufficiently thin samples. The main differences arise from the different penetration depths at 405 nm and 800 nm, followed by reabsorption of the PL light in the latter case, as illustrated in Fig. 1 (a). The detected PL emission $I(z, \lambda)$ from radiative recombination processes at a fixed distance z from the surface is $I(z, \lambda) = I(0, \lambda) \exp(-\alpha(\lambda) \cdot z)$. Here $\alpha(\lambda)$ is the absorption coefficient. Both the absorption length for two-photon absorption and the thickness of the crystal are longer than the linear absorption length in the spectral range under investigation. We thus create and collect TPI-PL for $z = 0$ to ∞ , and the detected spectrum can be approximated by

$$I_{\text{TPI-PL}}(\lambda) = I(0, \lambda) \int_0^\infty \exp(-\alpha(\lambda) \cdot z) dz = \frac{I(0, \lambda)}{\alpha(\lambda)} \quad (1)$$

Hence, if the PL spectrum at the surface $I(0, \lambda)$ is known, the absorption coefficient can be extracted from TPI-PL. We use the PL spectrum $I_{\text{PL}}(\lambda)$ with

405 nm excitation to estimate $I(0, \lambda)$. The ratio $I_{PL}(\lambda)/I_{TPI-PL}(\lambda)$ is given by green dots in Fig. 2 (a). The PL spectrum after 405 nm excitation, however, is itself subject to absorption [38, 52, 53], since carrier diffusion lengths in OIPS can exceed optical absorption lengths for photon energies above the band edge. Carriers hence recombine at finite distance from the surface, as illustrated in Fig. 1 (a). We account for the diffusion profile by integrating the PL intensity from different distances from the surfaces similar to Eq. 1. The finite diffusion length σ is modeled by introducing an additional term $\exp\left(-\left(\frac{z}{\sigma}\right)^2\right)$ in the integral. The corrected PL spectrum I_{PL}^{corr} is then given by

$$I_{PL}^{corr} = I_{PL} \left(\exp\left(\left(\frac{\alpha\sigma}{2}\right)^2\right) \operatorname{erfc}\left(\frac{\alpha\sigma}{2}\right) \right)^{-1}. \quad (2)$$

We first use Eq. 2 to calculate the corrected PL spectrum from the measured PL spectrum (blue) and the ratio (green) shown in Figs. 2 (a). The corrected PL spectra are given in Figs. 2 (b), (d). From these corrected spectra and the TPI-PL data the corrected absorption coefficient is then calculated using Eq. 1. Resulting absorption spectra are given in Figs. 2 (b), (c). While the exact line shape of the corrected spectra depends on the details of the model, the peak position at 2.29 eV in both absorption and emission is robust against changes in the diffusion profile, as long as $\alpha\sigma \geq 1$. This requirement is fulfilled since $1/\alpha = 90$ nm at 2.35 eV [39] and the diffusion length in OIPS single crystals is in the μm range [54, 55]. Corrected spectra in Fig. 2 are shown for $\alpha\sigma = 5$ at 2.35 eV photon energy. $\alpha\sigma = 5$ may be much longer because of photon recycling effects [56].

As proposed earlier [38, 39, 57], we model the absorption spectra $\alpha(E)$ using Elliot's theory [58, 59]:

$$\begin{aligned} \alpha(E) = & \frac{C_{A2}}{E^2} \frac{1 + \operatorname{erf}((E - E_{A2})/\gamma)}{1 - \exp(-2\pi^2 |E_{x1}/(E - E_{A2})|)} \\ & + \frac{C_{A1}}{E^2} \sum_{n=1}^3 (\gamma n^3)^{-1} \exp\left(-\left(\frac{E - (E_{A2} - E_{x1}/n^2)}{\gamma}\right)^2\right) \end{aligned} \quad (3)$$

The first term describes band absorption A2 with an onset at E_{A2} and amplitude C_{A2} , the second one excitonic enhancement A1 at E_{A1} with amplitude C_{A1} . γ is a broadening parameter, and $E_{x1} = E_{A2} - E_{A1}$ the exciton binding energy. Fits to the data are given as dark green lines in Fig. 2 (b). Fit results are summarized in Fig. 3.

The fits deviate from the absorption spectra systematically, as the measured spectra tail towards lower energy. Fit residua $\Delta\alpha(E)$ are given in Fig. 2 (c). We fit a power-law $\Delta\alpha(E) \propto (E - E_{A0})^n \theta(E - E_{A0})$ to

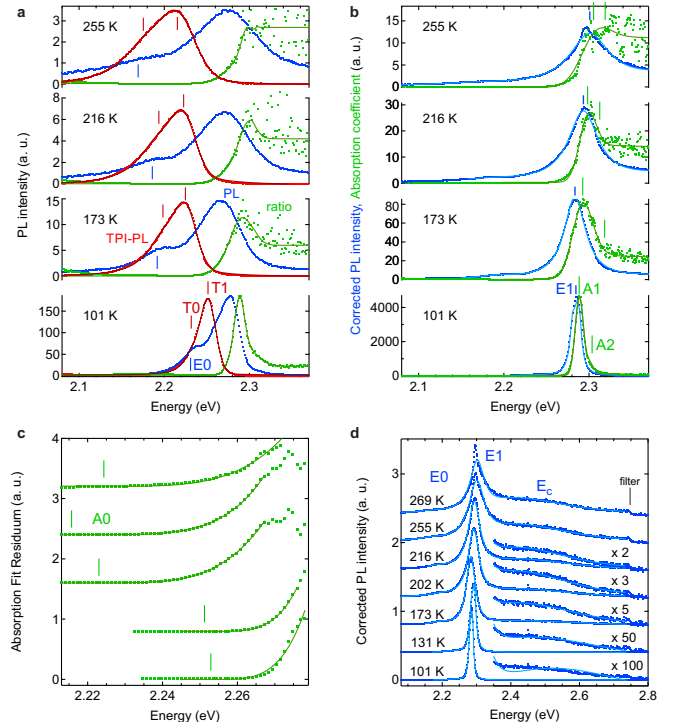


FIG. 2: (a) Photoluminescence spectra of single-crystal $(\text{CH}_3\text{NH}_3)\text{PbBr}_3$ after excitation with 405 nm light (blue) and 800 nm light (red), as well as their ratio (green). (b) gives the extracted absorption coefficients and photoluminescence spectra corrected for reabsorption, together with fits to the absorption coefficients. Fit residua are given in (c). (d) shows fits to the PL spectra over a wide energy range.

the residua, where E_{A0} is the position of the absorption onset A0 and $\theta(E)$ is Heavyside's theta function. The absorption onset lies energetically well above the emission from trap states identified from TPI-PL. Fits give $n = 4 \pm 0.5$, consistent with an indirect transition in combination with a low density of states (DOS) at the band edges of OIPS found in calculations [45, 60–62] and photoemission experiments [47, 63]. Power-law fits are shown as dark green lines in Fig. 2 (c), extracted E_{A0} are marked by ticks and summarized in Fig. 3 (a).

We now turn to the discussion of the PL spectra. As shown in Fig. 2 (a), (b), and (d), the (corrected) PL spectra exhibit three structures: a prominent peak E1 at 2.29 eV, a low-energy peak E0, and a high-energy continuum E_c . We use Lorentzian functions to fit E0 and E1. We attribute the continuum emission to free carriers, and take them into account in the fit by adding the function [64]

$$f_c(E)dE \propto (E - E_{E1})^2 \exp(-E/kT^*)dE \quad (4)$$

Where E_{E1} is the energetic position of the E1 emission feature, and $(E - E_{E1})^2$ reflects the joint density of states. Fits to the data are shown in Fig. 2 (c). The fit-

ting range is constrained by trap emission below 2.16 eV and the cutoff of the long-pass filter at 2.75 eV. We include free-carrier emission only in fits to the spectra of $(\text{CH}_3\text{NH}_3)\text{PbBr}_3$ in its tetragonal and cubic phase. Free carrier emission is weak at low temperature, in agreement with previous studies [28, 65]. The fitted exponential decay constant $kT^* \geq 0.06$ eV in Fig. 4, blue open squares in Fig. 3 (b), does not represent a thermodynamical temperature, but reflects a non-equilibrium distribution of carriers. The average energy $\langle E_c \rangle$ of the carriers is shown in Fig. 3 (a). For a parabolic density of states $\langle E_c \rangle = 3kT^*$, consistent with our data and ultrafast spectroscopies on $(\text{CH}_3\text{NH}_3)\text{PbI}_3$ [65]. For a square-root shaped DOS, in contrast, $\langle E_c \rangle = 1.5kT^*$. The low DOS at the band edges of OIPS provides one explanation for slow energy relaxation of carriers [11]. In time-correlated single photon counting from as-prepared $(\text{CH}_3\text{NH}_3)\text{PbBr}_3$ crystals, only a minor contribution of free carriers to the spectra was observed [28] as compared to their clear signature found here. The discrepancies probably arise from different surface preparations. We find intense free-carrier PL only after cleaving in UHV. The feature disappears after exposure to air, see Fig. 1 (b). $(\text{CH}_3\text{NH}_3)\text{PbBr}_3$ is extremely sensitive to gas adsorption [35], which can change surface band bending and trap state density, thus altering carrier diffusion and scattering.

The energetic positions of all spectral features are summarized in Fig. 3 (a): The prominent excitonic transition A1 (E1) at 2.29 eV is consistent with reflectance measurements [38, 48, 66] and almost independent of temperature. Its position matches the one reported for thinner crystals [28], in which diffusion and re-absorption play a minor role. The related exciton binding energy $E_{x1} = E_{A2} - E_{A1} = 22 \pm 2$ meV for $T \leq 200$ K is in agreement with the value of 25 ± 5 meV reported from low-temperature magnetoabsorption [23]. The position of the absorption onset A0, in contrast, changes from 2.25 eV in the low-temperature orthorhombic phase to around 2.22 eV at higher temperature. Its position matches the absorption onset found in transmission from the same crystals [47] and the onset reported from photoluminescence excitation [35]. The transition is accompanied by excitonic emission observed both in regular PL (E0) and TPI-PL (T0). In TPI-PL, additional emission (T1) occurs at higher energy, which we attribute to indirect band-edge emission. The energies of the phonons involved are small, since the transition is only slightly indirect and the velocity of sound is low in $(\text{CH}_3\text{NH}_3)\text{PbBr}_3$ [67]. The associated exciton binding energy $E_{x0} = E_{T1} - E_{T0}$ matches E_{x1} for $T \leq 200$ K. At higher temperature E_{x1} decreases, see Fig. 3 (b), as observed also for $(\text{CH}_3\text{NH}_3)\text{PbI}_3$ [16, 20, 22, 68, 69]. In contrast, E0 and T0 redshift, possibly due to a reduction of effective mass [15] and enhanced vibronic coupling, i. e. (multi-)phonon emission in the indirect emission process

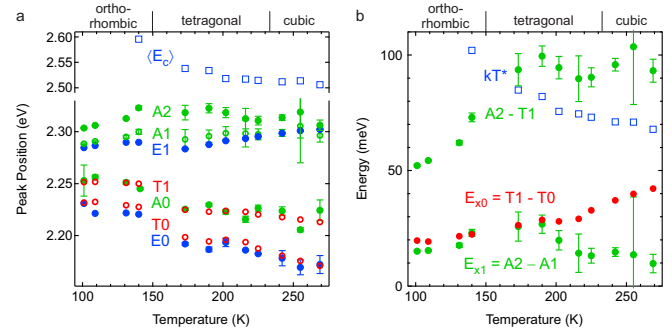


FIG. 3: Results of fits to PL data (blue), TPI-PL data (red) and extracted absorption spectra (green). (a) gives the extracted peak positions as discussed in the text and as labeled in Fig. 2. Selected peak spacings are shown by symbols in (b), together with the carrier quasi-temperature (open squares).

and large polaron formation [21, 25, 27, 28, 70].

The question arises, why the prominent direct transition is found several tens of meV above the band edge. The exact energy difference is given as A2–T1 in Fig. 3 (b). PL spectra similar to the ones presented here, with two emission peaks and a signature of free carriers, were measured on single-crystal $(\text{CH}_3\text{NH}_3)\text{PbI}_3$ at low temperature [71]. The authors assign the lower-energy emission peak to defects. In case of $(\text{CH}_3\text{NH}_3)\text{PbBr}_3$, the indirect transition lies energetically well above the defect emission at energies ≤ 2.16 eV identified from TPI-PL data. Moreover, photocurrent measurements showed that 2.18 eV excitation (matching the E0 and T0 energies) creates mobile charges in $(\text{CH}_3\text{NH}_3)\text{PbBr}_3$ at room temperature [72]. This process would be inefficient if optically active defect states needed to be excited initially, and then thermally activated to the bands related to the transitions around 2.3 eV. In a previous study [48], as-grown surfaces of single-crystal $(\text{CH}_3\text{NH}_3)\text{PbBr}_3$ were also investigated using a combination of TPI-PL and conventional PL. The authors assign low (high) energy emission to the bulk (surface) of the crystal. However, we find the low-energy E0 feature in regular PL, see Fig. 2 (a), demonstrating that the corresponding structure exists within ≈ 150 nm from the surface of a freshly-cleaved crystal. We point out that the absence of the E1 and E_c features in our TPI-PL data does not exclude that recombination of high-energy excitons and carriers takes place deep in the crystal, and that their luminescence signals get absorbed before they reach the surface. Indeed, the TPI-PL intensity reaches zero only for energies around 2.4 eV, indicating free-carrier recombination in the bulk.

Recently, a double-peak structure observed in PL from $(\text{CH}_3\text{NH}_3)\text{PbI}_3$ has been attributed to direct and indirect transitions in a Rashba-split band-structure [44]. Because of the similarity of the DOS of $(\text{CH}_3\text{NH}_3)\text{PbBr}_3$ to the one of $(\text{CH}_3\text{NH}_3)\text{PbI}_3$, a similar splitting is expected for $(\text{CH}_3\text{NH}_3)\text{PbBr}_3$. We recently found a signif-

icant Rashba splitting in photoemission experiments on $(\text{CH}_3\text{NH}_3)\text{PbBr}_3$ [47]. The Rashba energy is larger in the cubic than in the orthorhombic phase by a factor 1.5, in line with the current PL data. We thus conclude that we measure direct and indirect transitions in a Rashba system. The observation of a prominent above-gap direct transition explains thermally activated recombination [73], a photon-energy independent emission spectrum after band-gap excitation [74], and resulting optical refrigeration [6], as they were observed in related $(\text{CH}_3\text{NH}_3)\text{PbI}_3$ OIPS.

In summary, we combine bulk-sensitive two-photon induced photoluminescence and surface-sensitive conventional photoluminescence from $(\text{CH}_3\text{NH}_3)\text{PbBr}_3$ single crystals cleaved in UHV. The surfaces show broadband emission. The broad PL spectrum allows us to extract absorption spectra. They show a prominent direct transition at 2.31 eV, and an indirect transition at 2.25 eV (2.22 eV) in the orthorhombic (tetragonal) phase, each accompanied by excitonic emission. The spectra are consistent with a Rashba-split band structure. In addition, high-energy emission from free carriers centered around 2.5 eV is found from freshly cleaved single crystals. The feature disappears after exposing the crystals to air. The results underline the importance of environmental conditions in optical spectroscopy on OIPS, and represent a reference for surfaces prepared under ultra-clean conditions. The findings imply a slightly indirect band gap, which has been proposed as a source of long-lived carriers in OIPS [12, 14, 15].

* Electronic address: daniel.niesner@fau.de

- [1] W. S. Yang, J. H. Noh, N. J. Jeon, Y. C. Kim, S. Ryu, J. Seo, and S. I. Seok, *Science* **348**, 1234 (2015).
- [2] M. Saliba, S. Orlandi, T. Matsui, S. Aghazada, M. Cavazzini, J.-P. Correa-Baena, P. Gao, R. Scopelliti, E. Mosconi, K.-H. Dahmen, et al., *Nat. Energy* **1**, 15017 (2016).
- [3] S. D. Stranks and H. J. Snaith, *Nat. Nanotechnol.* **10**, 391 (2015).
- [4] L. Dou, Y. M. Yang, J. You, Z. Hong, W.-H. Chang, G. Li, and Y. Yang, *Nat. Commun.* **5**, 5404 (2014).
- [5] S. Yakunin, M. Sytnyk, D. Kriegner, S. Shrestha, M. Richter, G. J. Matt, H. Azimi, C. J. Brabec, J. Stangl, M. V. Kovalenko, et al., *Nature Photon.* **9**, 444 (2015).
- [6] S.-T. Ha, C. Shen, J. Zhang, and Q. Xiong, *Nature Photon.* **10**, 116 (2015).
- [7] H. Zhu, Y. Fu, F. Meng, X. Wu, Z. Gong, Q. Ding, M. V. Gustafsson, M. T. Trinh, S. Jin, and X. Y. Zhu, *Nat. Mater.* **14**, 636 (2015).
- [8] J. Even, L. Pedesseau, J.-M. Jancu, and C. Katan, *J. Phys. Chem. Lett.* **4**, 2999 (2013).
- [9] F. Brivio, K. T. Butler, A. Walsh, and M. van Schilfgaarde, *Phys. Rev. B* **89**, 155204 (2014).
- [10] C. Quarti, E. Mosconi, and F. De Angelis, *Chem. Mat.* **26**, 6557 (2014).

- [11] H. Kawai, G. Giorgi, A. Marini, and K. Yamashita, *Nano Lett.* **15**, 3103 (2015).
- [12] F. Zheng, L. Z. Tan, S. Liu, and A. M. Rappe, *Nano Lett.* **15**, 7794 (2015).
- [13] H. Mashiyama, Y. Kurihara, and T. Azetsu, *J. Kor. Phys. Soc.* **32**, S156 (1998).
- [14] T. Etienne, E. Mosconi, and F. De Angelis, *J. Phys. Chem. Lett.* **7**, 1638 (2016).
- [15] P. Azarhoosh, S. McKechnie, J. M. Frost, A. Walsh, and M. van Schilfgaarde, *APL Mater.* **4**, 091501 (2016).
- [16] J. Even, M. Carignano, and C. Katan, *Nanoscale* **8**, 6222 (2016).
- [17] A. N. Beecher, O. E. Semonin, J. M. Skelton, J. M. Frost, M. W. Terban, H. Zhai, A. Alatas, J. S. Owen, A. Walsh, and S. J. Billinge, *ACS Energy Letters* (2016).
- [18] O. Yaffe, Y. Guo, T. Hull, C. C. Stoumpos, L. Z. Tan, D. A. Egger, F. Zheng, O. E. Semonin, A. N. Beecher, T. F. Heinz, et al., *arXiv* preprint arXiv:1604.08107 (2016).
- [19] S. D. Stranks, V. M. Burlakov, T. Leijtens, J. M. Ball, A. Goriely, and H. J. Snaith, *Phys. Rev. Appl.* **2**, 034007 (2014).
- [20] J. Even, L. Pedesseau, and C. Katan, *J. Phys. Chem. C* **118**, 11566 (2014).
- [21] E. Menéndez-Proupin, C. L. Beltrán Ríos, and P. Wahnón, *Phys. Status Solidi RRL* **9**, 559 (2015).
- [22] A. Miyata, A. Mitioglu, P. Plochocka, O. Portugall, J. T.-W. Wang, S. D. Stranks, H. J. Snaith, and R. J. Nicholas, *Nat. Phys.* **11**, 582 (2015).
- [23] K. Galkowski, A. Mitioglu, A. Miyata, P. Plochocka, O. Portugall, G. E. Eperon, J. T.-W. Wang, T. Stergiopoulos, S. D. Stranks, H. J. Snaith, et al., *Energy Environ. Sci.*, **9**, 962 (2016).
- [24] D. Demchenko, N. Iziumskaya, M. Feneberg, V. Avrutin, Ü. Özgür, R. Goldhahn, and H. Morkoç, *Phys. Rev. B* **94**, 075206 (2016).
- [25] M. Bokdam, T. Sander, A. Stroppa, S. Picozzi, D. D. Sarma, C. Franchini, and G. Kresse, *Sci. Rep.* **6**, 28618 (2016).
- [26] Z.-G. Yu, *J. Phys. Chem. Lett.* **7**, 3078 (2016).
- [27] J. M. Frost and A. Walsh, *Acc. Chem. Res.* **49**, 528 (2016).
- [28] H. Zhu, K. Miyata, Y. Fu, J. Wang, P. P. Joshi, D. Niesner, K. W. Williams, and X.-Y. Zhu, *Science* **353**, 1409 (2016).
- [29] J.-S. Park, S. Choi, Y. Yan, Y. Yang, J. M. Luther, S.-H. Wei, P. Parilla, and K. Zhu, *J. Phys. Chem. Lett.* **6**, 4304 (2015).
- [30] G. Grancini, A. R. S. Kandada, J. M. Frost, A. J. Barker, M. De Bastiani, M. Gandini, S. Marras, G. Lanzani, A. Walsh, and A. Petrozza, *Nature photon.* **9**, 695 (2015).
- [31] J. Xing, X. F. Liu, Q. Zhang, S. T. Ha, Y. W. Yuan, C. Shen, T. C. Sum, and Q. Xiong, *Nano Lett.* **15**, 4571 (2015).
- [32] X. Wu, M. T. Trinh, D. Niesner, H. Zhu, Z. Norman, J. S. Owen, O. Yaffe, B. J. Kudisch, and X.-Y. Zhu, *J. Am. Chem. Soc.* **137**, 2089 (2015).
- [33] J. Dai, H. Zheng, C. Zhu, J. Lu, and C. Xu, *J. Mater. Chem. C* **4**, 4408 (2016).
- [34] D. Li, G. Wang, H.-C. Cheng, C.-Y. Chen, H. Wu, Y. Liu, Y. Huang, and X. Duan, *Nat. Commun.* **7**, 11330 (2016).
- [35] H.-H. Fang, S. Adjokatse, H. Wei, J. Yang, G. R. Blake, J. Huang, J. Even, and M. A. Loi, *Sci. Adv.* **2**, e1600534

(2016).

[36] C. Müller, T. Glaser, M. Plogmeyer, M. Sendner, S. Döring, A. A. Bakulin, C. Brzuska, R. Scheer, M. S. Pshenichnikov, W. Kowalsky, et al., *Chem. Mater.* **27**, 7835 (2015).

[37] K. Tanaka, T. Takahashi, T. Ban, T. Kondo, K. Uchida, and N. Miura, *Solid State Commun.* **127**, 619 (2003).

[38] Y. Yang, Y. Yan, M. Yang, S. Choi, K. Zhu, J. M. Luther, and M. C. Beard, *Nat. Commun.* **6**, 7961 (2015).

[39] Y. Yang, M. Yang, Z. Li, R. Crisp, K. Zhu, and M. C. Beard, *J. Phys. Chem. Lett.* **6**, 4688 (2015).

[40] M. A. Green, Y. Jiang, A. M. Soufiani, and A. Ho-Baillie, *J. Phys. Chem. Lett.* **6**, 4774 (2015).

[41] K. Zheng, Q. Zhu, M. Abdellah, M. E. Messing, W. Zhang, A. Generalov, Y. Niu, L. Ribaud, S. E. Canton, and T. Pullerits, *J. Phys. Chem. Lett.* **6**, 2969 (2015).

[42] J. Tilchin, D. N. Dirin, G. I. Maikov, A. Sashchiuk, M. V. Kovalenko, and E. Lifshitz, *ACS nano* **10**, 6363 (2016).

[43] R. T. Ross and A. J. Nozik, *J. Appl. Phys.* **53**, 3813 (1982).

[44] T. Wang, B. Daiber, J. M. Frost, S. A. Mann, E. C. Garnett, A. Walsh, and B. Ehrler, arXiv preprint arXiv:1609.07036 (2016).

[45] R. A. Jishi, O. B. Ta, and A. A. Sharif, *J. Phys. Chem. C* **118**, 28344 (2014).

[46] E. Mosconi, P. Umari, and F. De Angelis, *Phys. Chem. Chem. Phys.* (2016).

[47] D. Niesner, M. Wilhelm, I. Levchuk, A. Osvet, S. Shrestha, M. Batentschuk, C. Brabec, and T. Fauster, *Phys. Rev. Lett.* **117**, 126401 (2016).

[48] B. Wu, H. T. Nguyen, Z. Ku, G. Han, D. Giovanni, N. Mathews, H. J. Fan, and T. C. Sum, *Adv. Energy Mater.* **6** (2016).

[49] R. Ohmann, L. K. Ono, H.-S. Kim, H. Lin, M. V. Lee, Y. Li, N.-G. Park, and Y. Qi, *J. Am. Chem. Soc.* **137**, 16049 (2015).

[50] See Supplemental Material at [URL will be inserted by publisher] for experimental details of the TPI-PL measurements. Fig. 1 illustrates how excitation density and penetration depth were determined. Fig. 2 shows the TPI-PL intensity as a function of the laser repetition rate. Fig. 3 gives temperature-dependent intensities.

[51] G. Walters, B. R. Sutherland, S. Hoogland, D. Shi, R. Comin, D. P. Sellan, O. M. Bakr, and E. H. Sargent, *ACS nano* **9**, 9340 (2015).

[52] W. Tian, C. Zhao, J. Leng, R. Cui, and S. Jin, *J. Am. Chem. Soc.* **137**, 12458 (2015).

[53] T. Yamada, Y. Yamada, H. Nishimura, Y. Nakaike, A. Wakamiya, Y. Murata, and Y. Kanemitsu, *Advanced Electronic Materials* **2**, 1500290 (2016).

[54] Q. Dong, Y. Fang, Y. Shao, P. Mulligan, J. Qiu, L. Cao, and J. Huang, *Science* **347**, 967 (2015).

[55] D. Shi, V. Adinolfi, R. Comin, M. Yuan, E. Alarousu, A. Buin, Y. Chen, S. Hoogland, A. Rothenberger, K. Katsiev, et al., *Science* **347**, 519 (2015).

[56] L. M. Pazos-Outón, M. Szumilo, R. Lamboll, J. M. Richter, M. Crespo-Quesada, M. Abdi-Jalebi, H. J. Beeson, M. Vrućinić, M. Alsari, H. J. Snaith, et al., *Science* **351**, 1430 (2016).

[57] M. Saba, M. Cadelano, D. Marongiu, F. Chen, V. Sarritzu, N. Sestu, C. Figus, M. Aresti, R. Piras, A. G. Lehmann, et al., *Nat. Commun.* **5** (2014).

[58] R. Elliott, *Phys. Rev.* **108**, 1384 (1957).

[59] M. Feneberg, M. F. Romero, M. Röppischer, C. Cobet, N. Esser, B. Neuschl, K. Thonke, M. Bickermann, and R. Goldhahn, *Phys. Rev. B* **87**, 235209 (2013).

[60] P. Umari, E. Mosconi, and F. De Angelis, *Sci. Rep.* **4**, 4467 (2014).

[61] C. Motta, F. El-Mellouhi, S. Kais, N. Tabet, F. Alharbi, and S. Sanvito, *Nat. Commun.* **6**, 7026 (2015).

[62] E. Menéndez-Proupin, P. Palacios, P. Wahnmón, and J. C. Conesa, *Phys. Rev. B* **90**, 045207 (2014).

[63] J. Endres, D. A. Egger, M. Kulbak, R. A. Kerner, L. Zhao, S. H. Silver, G. Hodes, B. P. Rand, D. Cahen, L. Kronik, et al., *J. Phys. Chem. Lett.* **7**, 2722 (2016).

[64] Y. Varshni, *Phys. Status Solidi (b)* **19**, 459 (1967).

[65] D. Niesner, H. Zhu, K. Miyata, P. J. Joshi, T. J. Evan, B. J. Kudisch, M. T. Trinh, M. Marks, and X.-Y. Zhu, submitted (2016).

[66] H. Kunugita, T. Hashimoto, Y. Kiyota, Y. Udagawa, Y. Takeoka, Y. Nakamura, J. Sano, T. Matsushita, T. Kondo, T. Miyasaka, et al., *Chem. Lett.* **44**, 852 (2015).

[67] A. Létoublon, S. Paofai, B. Rufflé, P. Bourges, B. Hehlen, T. Michel, C. Ecolivet, O. Durand, S. Cordier, C. Katan, et al., *J. Phys. Chem. Lett.* **7**, 3776 (2016).

[68] Y. Yamada, T. Nakamura, M. Endo, A. Wakamiya, and Y. Kanemitsu, *IEEE J. Photovolt.* **5**, 401 (2015).

[69] H.-H. Fang, R. Raissa, M. Abdu-Aguye, S. Adjokatse, G. R. Blake, J. Even, and M. A. Loi, *Adv. Func. Mater.* **25**, 2378 (2015).

[70] J. Ma and L.-W. Wang, *Nano Lett.* **15**, 248 (2014).

[71] H. Diab, G. Trippé-Allard, F. Lédée, K. Jemli, C. Vilari, G. Bouchez, V. L. Jacques, A. Tejeda, J.-S. Lautret, E. Deleporte, et al., arXiv preprint arXiv:1606.01729 (2016).

[72] Y. Fang, Q. Dong, Y. Shao, Y. Yuan, and J. Huang, *Nature Photon.* **9**, 679 (2015).

[73] T. J. Savenije, C. S. Ponceca Jr, L. Kunneman, M. Abdellah, K. Zheng, Y. Tian, Q. Zhu, S. E. Canton, I. G. Scheblykin, T. Pullerits, et al., *J. Phys. Chem. Lett.* **5**, 2189 (2014).

[74] C. Wehrenfennig, M. Liu, H. J. Snaith, M. B. Johnston, and L. M. Herz, *J. Phys. Chem. Lett.* **5**, 1300 (2014).